PHILOSOPHICAL TRANSACTIONS OF THE ROYAL SOCIETY A MATHEMATICAL, PHYSICAL & ENGINEERING SCIENCES

Inertial-confinement fusion with fast ignition

O. Willi

Phil. Trans. R. Soc. Lond. A 1999 **357**, 555-574
doi: 10.1098/rsta.1999.0341

THE ROYAL SOCIETY

Inertial-confinement fusion with fast ignition

By O. Willi

Department of Physics, Imperial College of Science, Technology and Medicine, Prince Consort Road, London SW7 2BZ, UK

The fast ignitor scheme consists of three stages and relies on ignition of a part of the compressed fusion fuel of an inertial-confinement fusion capsule by an external trigger. A conventional fusion target is imploded uniformly either by a soft X-ray or laser pulse. A hole is bored through the corona plasma resulting in a channel that leads to the edge of the compressed core. This channel is produced by the ponderomotive force and relativistic effects of a high intensity laser pulse with a duration of tens of picoseconds. Finally, an ultraintense picosecond laser pulse is guided through the channel to the critical density and converted to an MeV electron beam. The electron beam then propagates from the critical density to the high-density core igniting the compressed fusion fuel. As a lower compression ratio is required with this scheme the uniformity of driver and the symmetry requirements of the implosion are less stringent. There are, however, several critical plasma and laser physics issues involved in this scheme, including hole boring, electron-beam generation and propagation and the production of a laser pulse with a duration of 1–10 ps and an energy between 10 and 100 kJ.

Keywords: fast ignition; laser fusion; relativistic laser–plasma interaction; relativistic channelling; inertial fusion energy; hole boring

1. Introduction

With the present construction of the National Ignition Facility (NIF) (Kilkenny *et al.*, this issue), the possibility of inertial fusion energy has moved a step closer. In particular, it is projected that ignition of a spherical capsule filled with deuterium–tritium (D–T) will be achieved with the NIF by using conventional inertial-confinement fusion (ICF). This relies on the formation of a hot central core within the dense fuel to spark ignition. This is achieved by a rapid, highly symmetric spherical implosion of a capsule driven by a temporally shaped multi-nanosecond laser or soft X-ray pulse. Present simulations predict that a gain of about 10 will be achieved with the NIF. Because of the extreme requirements on symmetry (less than 1%) and the necessity to achieve both high temperature and density in the implosion, conventional ICF requires substantial energy (more than 1 MJ of laser energy) to achieve ignition and thermonuclear burn. For a fusion power plant, gains above 100 are required due to the relatively low driver and hydrodynamic efficiencies (Kidder 1979). For these reasons, Tabak *et al.* (1994) have recently proposed the fast ignitor scheme. This new concept requires the delivery of an intense, multikilojoule pulse to the dense precompressed fuel core (density *ca.* 300 g cm^{-3}) within a few picoseconds. The fast ignition scheme involves hole boring into the overdense plasma and the generation of relativistic electrons that ignite the precompressed fusion fuel. Such external ignition strongly relaxes driver and target requirements and may produce a higher gain

with less driver energy. The physical processes in this novel regime are not yet well understood. Extreme conditions exist with light pressure of many gigabars, electric fields much larger than the Coulomb field in an atom and strong relativistic effects. In addition, self-generated magnetic fields of hundreds of megagauss are predicted by simulations causing collimation of the relativistic electrons into a beam and strongly modifying the thermal transport.

Although there are presently no plans to build a fast ignitor system on the NIF, the possibility of higher gain at lower driver energies merits further investigation. If the present studies show that this scheme is promising then a relatively low-cost upgrade of a short pulse capability could be installed on the NIF. Similar short pulse systems have been successfully added to NOVA, VULCAN and GEKKO laser systems and the NIF has been designed with enough flexibility in the beam arrangement to also allow this possibility.

This paper reviews some of the relevant physics issues of the fast ignitor concept and summarizes the work that has recently been carried out in this exciting and novel area of research.

2. Ignition models

In ICF the high densities required are obtained by using laser or soft X-ray ablation to compress a spherical capsule filled with D–T fuel (Nuckolls *et al.* 1972). The capsule is irradiated uniformly to compress the target up to densities of the order of $1000\ \mathrm{g\,cm^{-3}}$. The confinement time of a sphere of hot plasma is determined by the inertia, and is proportional to the radius divided by the sound speed. Consequently, in ICF, a requirement equivalent to the Lawson criterion can be expressed as a function of the fuel areal density ρR, where ρ is the density and R the radius of the compressed fuel.

A necessary condition for efficient energy production by ICF is a large energy gain, defined as the ratio $G = E_{\mathrm{th}}/E$ of the thermonuclear energy E_{th} released by the target to the energy E of the driver pulse. Often, different aspects of the target history are modelled separately. In particular, one can consider independently the stages of target implosion, leading to the production of a compressed fuel assembly, and the subsequent stages of ignition and thermonuclear burn. The burn performance is characterized by the so-called 'fuel gain' G_{F}, defined as the ratio of the thermonuclear energy to the initial internal energy of the compressed fuel, i.e. (Atzeni 1995)

$$G_{\mathrm{F}} = \frac{m\Phi Y_{\mathrm{D\text{–}T}}}{E_{\mathrm{D\text{–}T}}},$$

where m is the mass of the D–T fuel, Φ is the fraction of burned mass and $Y_{\mathrm{D\text{–}T}} = 3.34 \times 10^{18}\ \mathrm{erg\,g^{-1}}$ is the D–T yield, i.e. the energy released by the thermonuclear burn in unit mass of D–T.

The simplest ignition configuration is that of volume ignition in which ignition takes place throughout the full volume of a uniform compressed spherical fusion fuel. Higher gain can be achieved with spark ignition, which is regarded as the conventional approach to ICF. In this approach, the capsule containing the fusion fuel is compressed by a multi-nanosecond shaped pulse. A series of converging shocks is produced compressing and heating a small fraction of the fuel to ignition temperatures. Ignition occurs in the hot spot followed by a burn wave propagating outwards

through the fuel. This kind of compression produces an isobaric configuration, i.e. in which the high-temperature, low-density core and the surrounding high-density, low-temperature fuel are in pressure equilibrium. In the isobaric model, the hot spot is treated as a perfect gas, while the cold fuel is treated as a partly degenerate electron gas with α the degeneracy parameter. The maximum fuel gain which can be achieved with a given fuel energy $E_{\mathrm{D-T}}$ and α, is given by (Atzeni 1995; Meyer-ter-Vehn 1982)

$$G_{\mathrm{F}} = 5.6 \times 10^3 \left(\frac{E_{\mathrm{D-T}}\ [\mathrm{MJ}]}{\alpha^3} \right)^{0.3}$$

(for initial hot spot parameters of $T_0 = 5\,\mathrm{keV}$ and $\rho_0 r_0 = 0.4\,\mathrm{g\,cm^{-2}}$).

The most critical issues in conventional ICF are the symmetry and stability of capsule implosion. The asymmetry of the capsule must not exceed 1–2% to achieve the values of radial convergence required to generate the hot spot in the centre of the target (Meyer-ter-Vehn 1997). Also, ICF capsule implosions are subject to hydrodynamic instabilities such as the Rayleigh–Taylor instability (RTI) (Taylor 1950), since a low-density ablating plasma is driving a shell of higher density. The capsules have therefore to be fabricated with a very smooth surface. RTI is also a critical issue during the stagnation phase (i.e. when the imploding high-density shell is decelerated by central low-density fuel), as it tends to mix the highly compressed cold fuel with the hot spot, degrading the implosion.

3. Fast ignitor concept

The scheme proposed by Tabak *et al.* (1994) consists of three phases. In the first step, the spherical target filled with fuel is compressed by using the conventional ICF techniques to densities up to $300\,\mathrm{g\,cm^{-3}}$. A laser pulse with an intensity between 10^{17} and $10^{19}\,\mathrm{W\,cm^{-2}}$ and duration of 100 ps is then used to create a channel through the corona plasma. Finally, a 1–10 ps laser pulse is guided through the channel at an intensity of $10^{20}\,\mathrm{W\,cm^{-2}}$ to the compressed core. The pulse is absorbed, and its energy transferred to energetic electrons with an energy between 1 and 5 MeV. The mean free path of these electrons is such that they deposit their energy within a small distance of the absorption region. The heated deuterium and tritium ions in this region fuse and α-particles are produced. A burn wave then propagates into the cold compressed matter fusing the remaining fuel. Figure 1 shows a schematic of the various stages of fast ignition.

The ideal size of the hot spot is determined by the necessity of heating the core within an alpha-particle range, given by a ρR of about $0.3\,\mathrm{g\,cm^{-2}}$. With the fuel density of $300\,\mathrm{g\,cm^{-3}}$ a hot spot radius of 10 μm is required. The ignition pulse has to be shorter than the disassembly time of the fuel, resulting in a pulse of about 10 ps at these temperatures and radii. A lower limit for the pulse duration is set by the collision time between the electron and the ions, typically of the order of 1 ps.

If a method can be found to deliver the ignition energy sufficiently rapidly at the end of the compression stage of the pellet, the gain can be calculated using an isochoric (uniform density) model (Kidder 1976). A hot spot is created at the centre of the pellet with the density uniform throughout the pellet and hot spot, and cold fuel will be out of pressure equilibrium. It has been shown that the maximum gain attainable for central ignition for isochoric initial conditions is considerably higher than that for isobaric initial conditions (Tabak *et al.* 1994; Atzeni 1995). For

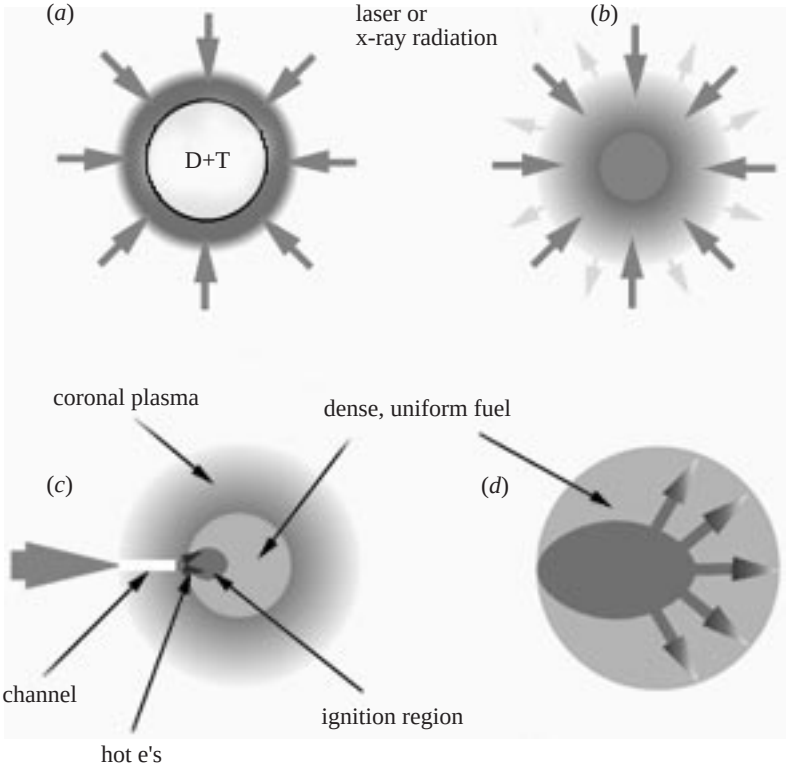

Figure 1. Schematic of the various stages of the fast ignition scheme for ICF. (*a*) 'Standard' implosion, (*b*) compression phase, (*c*) fast ignition, and (*d*) thermonuclear burn spreads through the compressed D–T.

example, Atzeni's recent estimate gives, for initial hot-spot parameters $T_0 = 12$ keV and $\rho R = 0.5\ \mathrm{g\ cm^{-2}}$,

$$G_{\mathrm{F}} = 1.92 \times 10^3 \left(\frac{E_{\mathrm{D\text{–}T}}\ [\mathrm{MJ}]}{\alpha} \right)^{0.4}.$$

This idea is at the centre of the fast ignitor concept. This novel scheme has been one of the main motivations behind the short laser pulse interaction research of the last few years. The essential idea behind this scheme is to assemble the fuel with sufficient density to sustain fusion burn but with a low and uniform temperature (a few hundred electronvolts). At the point of maximum compression of about $300\ \mathrm{g\ cm^{-3}}$ the ion temperature is rapidly increased to ignition conditions (5–10 keV) by an external relativistic electron beam trigger. Figure 2 shows a schematic of the different ignition schemes.

If the heating of the core reaches 10 keV, the energy that must be delivered to the core can be roughly estimated as $30(\rho^*)^{-2}$ kJ (Tabak *et al.* 1994), where $\rho^* = \rho/(100\ \mathrm{g\ cm^{-3}})$. This gives $E = 3$ kJ for the conditions mentioned above, corresponding to a minimum power requirement of the order of 0.3 PW. If one assumes perfect coupling between suprathermal electrons and compressed fuel, these values refer to the suprathermal electrons produced by the igniting pulses. The required laser energy will scale as $1/\eta$, where η is the efficiency of the conversion of the laser

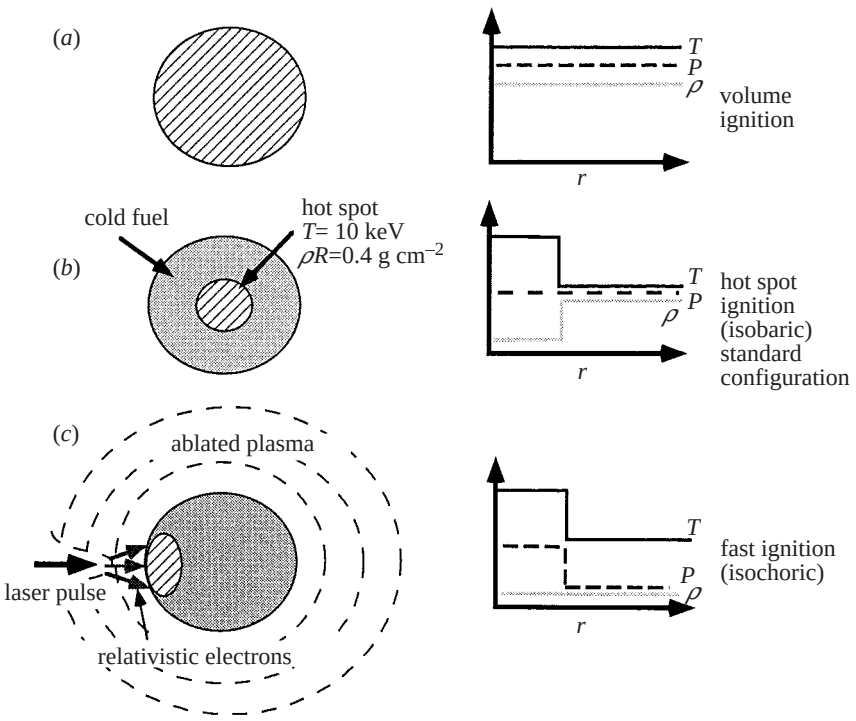

Figure 2. Schematic of different models for fuel ignition in ICF. (*a*) Volume ignition, (*b*) isobaric configuration with central hot spot, and (*c*) fast ignitor concept.

energy into MeV electrons. So far conversion efficiencies from the laser energy to hot electrons between 5 and 50% have been observed for irradiances between 10^{18} and 4×10^{19} W cm^{-2}. Recent three-dimensional (3D) PIC simulations (Pukhov & Meyer-ter-Vehn 1997) and initial experimental results indicate that laser intensities up to 10^{20} have to be used in order to produce an MeV electron temperature. At these intensities, relativistic effects have to be taken into account, and a whole new range of physical processes opens up. It has to be said that the original estimates by Tabak *et al*. now seem optimistic when compared to other authors' more recent predictions. For example, 2D simulations by Atzeni *et al*. (1997) with off-centre ignition indicate that the energy to be delivered to the core scales as $140(\rho^*)^{-1.85}$ kJ. Obviously, this would impose even stricter requirements on the ignitor pulse. The simulations show that for ignition to occur a total electron beam energy of about 20 kJ is required for a compressed D–T sphere with a density of 300 g cm^{-3}. In addition, Atzeni also considered a cylindrical fuel geometry to increase the target gain. In addition, with the very large predicted target gains for fast ignition deuterium targets with a very small seed of tritium content in the trigger region have been considered to lower the flux of the 14.06 MeV neutrons (Atzeni & Ciampi 1997).

As mentioned above, a potential advantage of fast ignition over conventional ICF schemes is the higher energy gain that can be achieved with smaller driver energy. Computational predictions show that gains of a few hundred can be obtained with energies similar to the NIF. Another advantage is that external ignition is expected to work at a reduced level of implosion symmetry compared with standard ICF. In fact,

calculations indicate that the fuel assembly should be much less sensitive to laser light non-uniformities and growth of hydrodynamic instabilities than the conventional ICF scheme (Tabak *et al.* 1994). In the fast ignitor scheme the difficulties are transferred to the development of a multi-kilojoule picosecond laser system and the production of a relativistic electron beam and its transport to the precompressed fuel core.

In order to test the feasibility of fast ignition, several plasma physics issues have to be investigated including

(1) the formation of a stable channel in the underdense and overdense regions of the plasma,

(2) the guiding of an ultraintense laser pulse through the channel,

(3) the absorption of the laser energy at the end of the channel and its conversion into MeV electrons, and

(4) the transport of the electron beam into the dense plasma core and the deposition of its energy.

4. Channel formation and hole boring

The formation of a stable channel in the underdense and overdense corona plasma is essential for the fast ignitor scheme. The distance that a Gaussian pulse can traverse before diffraction reduces the intensity is characterized by the Rayleigh length Z_{R}:

$$Z_{\mathrm{R}} = \pi\sigma_0^2/\lambda,$$

where σ_0^2 is the $1/e^2$ laser spot size defined for a Gaussian beam and λ is the laser wavelength. For typical laser parameters of $r_0 = 10\,\mu\mathrm{m}$, and $\lambda = 1\,\mu\mathrm{m}$, $Z_{\mathrm{R}} = 300\,\mu\mathrm{m}$. If the propagation of larger distances is required, the formation of a channel in the plasma is required. There are several processes that lead to channel formation, in particular self-focusing due to ponderomotive and relativistic effects. At very high intensities the pressure of the laser pulse P_{L} is extremely high, much larger than the thermal pressure of the plasma, and tends to push back the critical density surface. $P_{\mathrm{L}} = 2I/c \sim 600I/10^{18}$ Mbar, where I is the intensity in W cm^{-2}. Two-dimensional PIC simulations show that at an irradiance of 10^{19} W cm^{-2} the critical surface can be pushed back at a rate of 1/40th of the speed of light effectively boring a hole into the overdense plasma as observed by Wilks *et al.* (1992).

At relativistic intensities, both relativistic and ponderomotive effects will cause the laser pulse to self-focus. Indeed, the combination of these two effects can guide the pulse through the plasma over a distance of many Rayleigh lengths.

(*a*) *Ponderomotive channelling*

The ponderomotive force (F_{p}) can induce self-focusing from expulsion of electrons from the laser spot region due to the spatial variation across the laser beam profile. The ions follow due to space charge effects. The critical density surface can also be pushed back into the target due to the F_{p} at the leading edge of the pulse. The F_{p} is given by (Chen 1984)

$$F_{\mathrm{p}} = -\frac{\omega_{\mathrm{p}}^2}{\omega_0^2}\frac{\nabla\langle E\rangle^2}{8\pi},$$

where ω_p and ω_0 are the plasma and laser frequencies, respectively.

At relativistic intensities the $F_{p,rel}$ is given by

$$F_{p,rel} = -m_e c^2 \nabla(\gamma - 1),$$

where m_e is the electron mass, c is the speed of light and γ is the relativistic factor (Kruer & Wilks 1994).

The density depression on the axis can evolve into a plasma channel. Two different cases need to be distinguished. If the pulse is very short, ion inertia prevents significant motion of ions occurring during the duration of the light pulse. In this case the expulsion of the electrons will lead to a charge imbalance, creating an electrostatic field that attracts the electrons back into the channel. The balance between electrostatic and ponderomotive force determines the electron density within the channel. It has been predicted that the ponderomotive force may lead to complete expulsion of electrons within some inner core radius of the laser beam channel (of the order of c/ω_{pe}) if the laser power P overcomes a threshold value P_c (Sun *et al.* 1987). If the ions do not move, the channel does not outlive the laser pulse, as the space-charge force will pull back the electrons as soon as the ponderomotive force is turned off.

The situation changes if the pulse is sufficiently long to allow motion of the ions to take place while the pulse is on. In this case, a fraction of the ions follow the electrons due to the space-charge force. Being accelerated by the space-charge, the ions acquire large outward radial velocities, and continue to drift radially even after the passage of the laser pulse. The expansion of the channel after the interaction has been described as a *Coulomb explosion* (Burnett & Enright 1990).

The formation of a channel with ion cavitation has been observed in several PIC simulations. Among these, Mori reported complete evacuation of ions and electrons in 2D simulations performed in a very underdense plasma (Mori *et al.* 1988). Three-dimensional simulations of the propagation of a pulse at irradiance 10^{19} W cm^{-2} in a near critical plasma also showed channel formation with almost complete cavitation (Pukhov & Meyer-ter-Vehn 1996). In this simulation, ions were accelerated radially due to the electrostatic field set up by the charge separation, reaching energies up to 3 MeV.

Independently from the mechanisms through which the laser energy is transferred to the plasma, the expansion of the channel after the laser pulse propagation can be seen as the evolution of a cylindrical blast wave following a strong explosion in a gas; a situation widely studied in gas dynamics theory. In this treatment, the transfer of energy from the laser to the plasma is seen as the instantaneous release of a finite amount of energy at the centre of symmetry (in this case the laser axis). Following the explosion, a cylindrical disturbance propagates through the gas. The disturbed gas region is separated from the undisturbed region (where pressure and density stay at the initial values) by a discontinuity, i.e. a shock. This physical process has been studied by Sedov (1959).

(*b*) *Relativistic channelling*

At the very high intensities the physics of the interaction changes drastically due to the fact that the quiver velocity v_{osc} of the electrons oscillating in the laser electric field approaches the speed of light,

$$\frac{v_{osc}}{c} \approx 0.84 \left(\frac{I\lambda^2}{10^{18}\ \mathrm{W\ cm^{-2}\ \mu m^2}} \right)^{1/2},$$

where c is the speed of light, I is the laser irradiance and λ is the laser wavelength (Gibbon & Förster 1996). Consequently, for $I\lambda^2 > 10^{18}\,\mathrm{W\,cm^{-2}\,\mu m^2}$, relativistic effects have to be taken into account.

At relativistic intensities the refractive index of the plasma becomes intensity dependent. This results in an increase of the effective critical density (Sprangle *et al.* 1992). The effective critical density n_c^{eff} is given by

$$n_c^{\mathrm{eff}} = \gamma n_c \approx n_c\left(1 + \frac{I\lambda^2}{3\times 10^{18}\,\mathrm{W\,cm^{-2}\,\mu m^2}}\right)^{1/2}.$$

At sufficiently extreme intensities, this can lead to *induced transparency*, where the laser beam is transmitted through a nominally overdense plasma instead of being reflected (Kaw & Dawson 1970). It follows that the refractive index is higher in the regions where the electromagnetic radiation is more intense. If the laser has, for example, a Gaussian intensity profile, the refractive index will have a maximum on the propagation axis, acting like a positive lens. This causes *relativistic self-focusing*. The power threshold for relativistic self-focusing is given by

$$P_c\,[\mathrm{GW}] = 17.4(\omega_0/\omega_p)^2,$$

where ω_p and ω_0 are the plasma and laser frequency, respectively. Relativistic self-focusing and channelling is an alternative method for guiding the pulse as the pulse relativistically modifies the plasma refractive index to overcome diffraction. The laser pulse can be guided over many Rayleigh lengths.

(*c*) *Magnetic self-channelling*

Recently, 2D and 3D PIC simulations (Pukhov & Meyer-ter-Vehn 1996) predicted another mechanism that can lead, together with the relativistic and ponderomotive processes, to the formation of a stable channel during the propagation of an ultra-intense laser pulse through a plasma. The key feature observed in these simulations, performed for laser powers well above the relativistic threshold, was that, similarly to previous predictions for interactions with overdense plasmas, the laser pulse drives along the propagation direction a current of relativistic electrons.

Computational results indicate that extremely large magnetic fields are generated during the propagation of an ultraintense laser pulse through a dense plasma (Pukhov & Meyer-ter-Vehn 1996, 1997; Wilks *et al*. 1992; Mason & Tabak 1998). Since these fields may have an effect on the laser pulse propagation and the transport of the fast electron energy, the study of magnetic field generation in ultraintense laser–plasma interaction has to be regarded as a fundamental issue.

Due to the plasma quasi-neutrality, the average current of these fast electrons must be cancelled by a return current carried by electrons of the cold plasma component. The currents in the opposite direction repel each other, leading to the onset of the Weibel instability (Weibel 1959), which makes the distribution of the current density inhomogeneous in the transverse direction. The electron current breaks up, forming filaments of fast electrons moving forward and spatially separated from the colder return current (Forslund 1985; Pegoraro *et al.* 1996).

An important point is that the laser light 'follows' the path of the relativistic electrons. In fact, the concentration of fast electrons into filaments determines a local decrease of the index of refraction. This causes the laser beam to filament

following the path of the electron beamlets (this filamentation process is equivalent to relativistic self-focusing). This large electron current produces large magnetic fields. Magnetic fields with amplitudes of more than 100 MG have been observed in PIC simulations.

The filamentary electron currents attract each other, via their large self-generated magnetic fields (Askar'yan *et al.* 1995). Eventually, the currents (and consequently the light filaments) merge together, leading to laser propagation into a single filament and to a relativistic electron beam propagating with the laser pulse. A large toroidal magnetic field, generated by the electron current, surrounds the channel confining the electron beam. As a result, the laser pulse propagates in a channel with a radius of the order of the laser wavelength.

The simulations reported in (Pukhov & Meyer-ter-Vehn 1996) were performed for a laser pulse with an intensity of 1.2×10^{19} W cm^{-2}, propagating in an homogeneous underdense plasma with a density of $0.36n_c$. With these parameters the interaction was followed up to 320 fs after the interaction. A population of fast electrons accelerating forward was observed, with an energy spectrum resembling a thermal distribution corresponding to temperatures of the order of 3–5 MeV. The corresponding current was of the order of 10 kA, generating a toroidal magnetic field in the range 50–100 MG. Ion cavitation, due to the space-charge following the ponderomotive expulsion of the electrons was also observed, and, together with the relativistic modifications of the refractive index, contributed to the channelling of the pulse.

The formation of stable channels in underdense, near-critical plasmas has been observed in several experiments, using sub- and picosecond pulses (Borghesi *et al.* 1997; Young & Bolton 1996; Krushelnick *et al.* 1997; Wagner *et al.* 1997; Fuchs *et al.* 1998). The channel forms due to ponderomotive expulsion of electrons and survives long after the passage of the pulse. If the pulse is sufficiently intense, relativistic effects also have an important role in the channelling process. Guiding of a second pulse, at intensities up to 5×10^{16} W cm^{-2}, through the preformed channel has also been demonstrated (Krushelnick *et al.* 1997).

Figure 3*a* shows a 2ω time-integrated self-emission image ($\lambda = 0.527$ μm) generated by a 1 ps, 1.054 μm laser pulse at an irradiance of 3×10^{18} W cm^{-2} that interacted with a preformed plasma. Figure 3*b* shows a snapshot of a 3D PIC simulation of the self-focused laser pulse after 0.5 ps (Borghesi *et al.* 1997). The shaded surface corresponds to 67% of $\langle I_{\max} \rangle$. It can be seen from interferometric measurements that the laser pulse focuses down to 5 μm in size at a density of around 0.05 times the critical density n_c ($n_c \sim 1 \times 10^{21}$ cm^{-3} for $\lambda = 1$ μm). It should also be noted that, at this density, the laser power of 10 TW was about 25 times the threshold power for relativistic self-focusing. $P_c \approx 0.4$ TW for a density of $0.05n_c$. The channel width pulsates as the laser defocuses and refocuses with a characteristic period of $15–30\lambda$ qualitatively in agreement with the simulations.

Figure 4*a* shows an interferogram recorded at 60 ps after the interaction of a CPA pulse with a preformed plasma. It is evident that the laser-induced density depression persists even long after the pulse. The temporal evolution of the density channel structure was studied in a series of interferograms recorded at different times. In figure 4*b*, the channel radius size is plotted versus time on a log–log scale. The data was fitted with the self-similar analytical solution for a cylindrical blast wave (Sedov 1959). The data were very well described by the function $R(t) = K(t - t_0)^{1/2}$, that is the self-similar solution with the time-axis shifted by $t_0 = 1.8$ ps (with K a

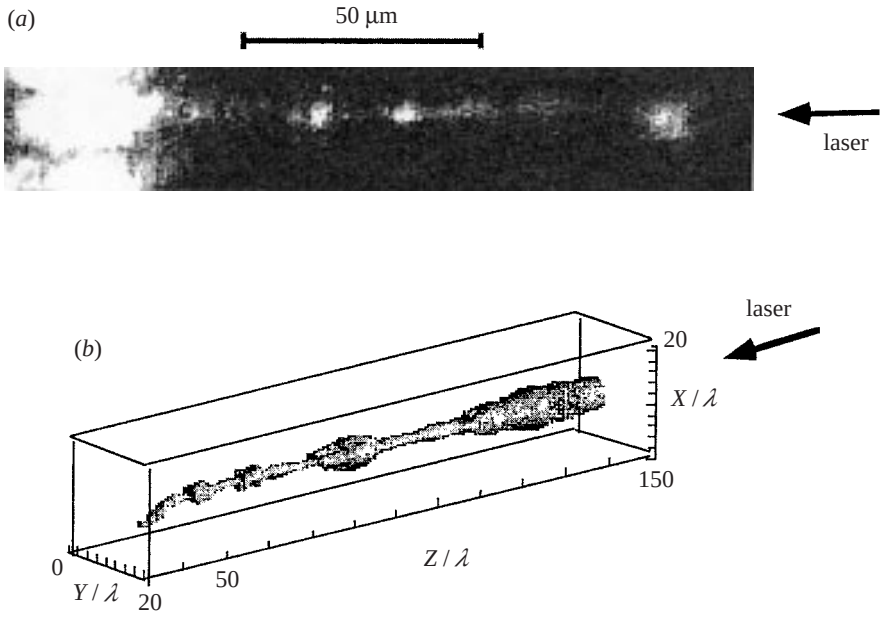

Figure 3. Self-focusing of a 10 TW, 1 ps, 1 µm pulse in a near-critical preformed plasma. The pulse was focused at an irradiance of 3×10^{18} W cm^{-2}. (*a*) Second-harmonic emission channel. (*b*) 3D PIC code simulation: snapshot at the peak of the laser pulse. The shaded surface corresponds to 67% of $\langle I_{\max}\rangle$.

constant of the order of $(E_0/\rho_0)^{1/4}$, where E_0 is the energy deposited in the plasma per unit length and ρ_0 the unperturbed density). The shift t_0 is comparable with the temporal uncertainty of the measurements. Also, it is reasonable to assume that the similarity solution does not hold in the first few picoseconds, when the plasma has not yet reached local thermal equilibrium.

The magnetic fields induced by the relativistic electrons and the conventional thermal electric magnetic field have recently been observed in a preformed plasma using optical Faraday rotation (Borghesi *et al.* 1998*a*). Figure 5 shows the analysis of a Faraday rotation image. The rotation angle inversion is clearly visible in a lineout from the experimental data. The value of the outer rotation (about 2°) suddenly decreases by almost 3° approaching the laser axis as seen in figure 5*a*. The corresponding lineout for the product nB, extracted by Abel inversion, is shown in figure 5*b*. From the plot it is evident that the abrupt changes in the rotation angle observed in the data corresponds to an inversion of the magnetic field direction. A value for the outer magnetic field can be extracted from the corresponding rotation, dividing the product nB by the density n of the preformed plasma. This gives an amplitude of about 1 MG for the thermal electric field. In order to better understand the inner magnetic field observations, it is worth remembering here that in these experimental conditions the pulse undergoes relativistic self-channelling. An evacuated channel is formed during the interaction due to the combined effect of ponderomotive expulsion of the electrons and subsequent motion of the ions due to the strong space-charge field. Even after the laser pulse is turned off, the channel structure keeps expanding. The amplitude of the field inside the channel can be esti-

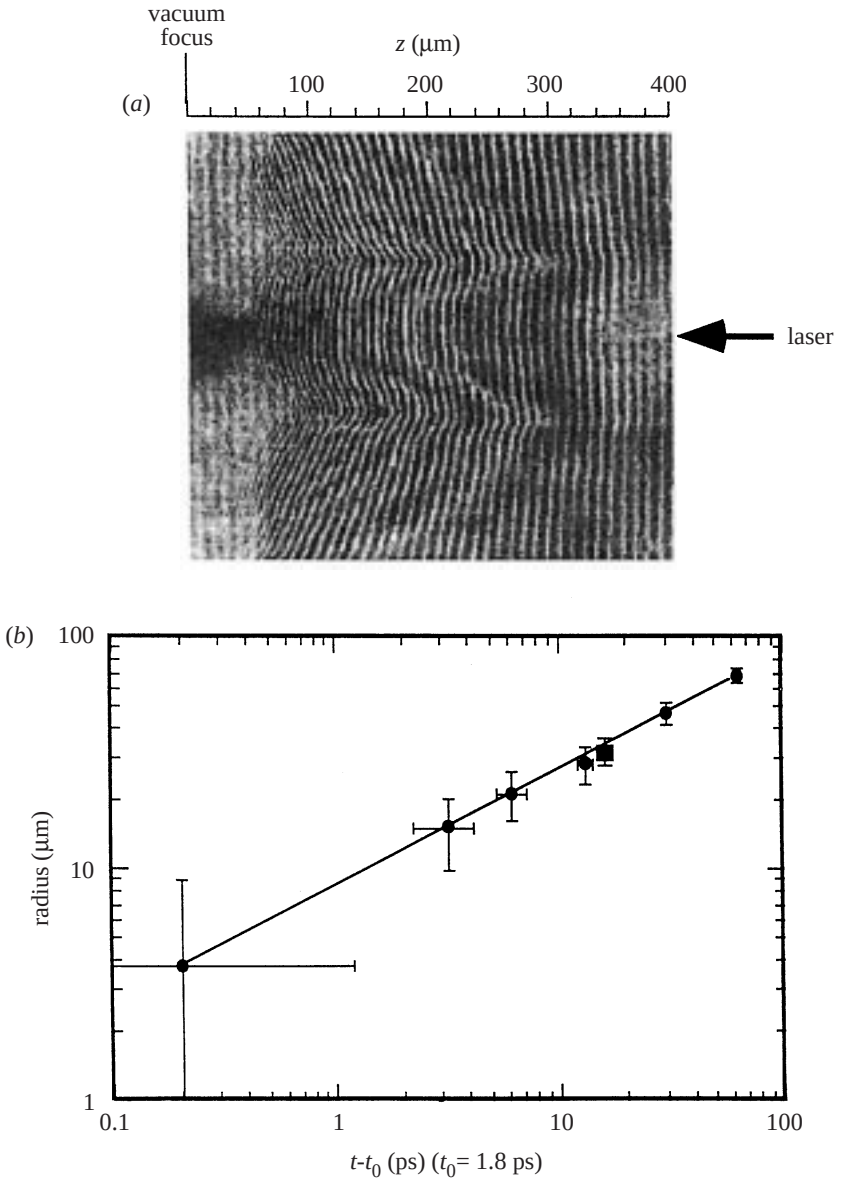

Figure 4. (*a*) Interferogram recorded 60 ps after the interaction of the CPA pulse with the preformed plasma. (*b*) Temporal evolution of the channel radius in the plasma ($t_0 = 1.8$ ps). The solid line represents the best fit of the data using the function $R = K(t - t_0)^{1/2}$.

mated from figure 5*b*. Values in the range 5–10 MG are obtained if one considers n_{in} to be of the order of 0.1–0.5n_0, where n_{in} is the density inside the channel and n_0 is the background density of the preformed plasma. The interaction was studied, under conditions close to those of the reported experiment, using the 3D PIC code VLPL. A large toroidal magnetic field surrounding the laser axis is observed, in correspondence with a current of relativistic electrons travelling with the laser pulse.

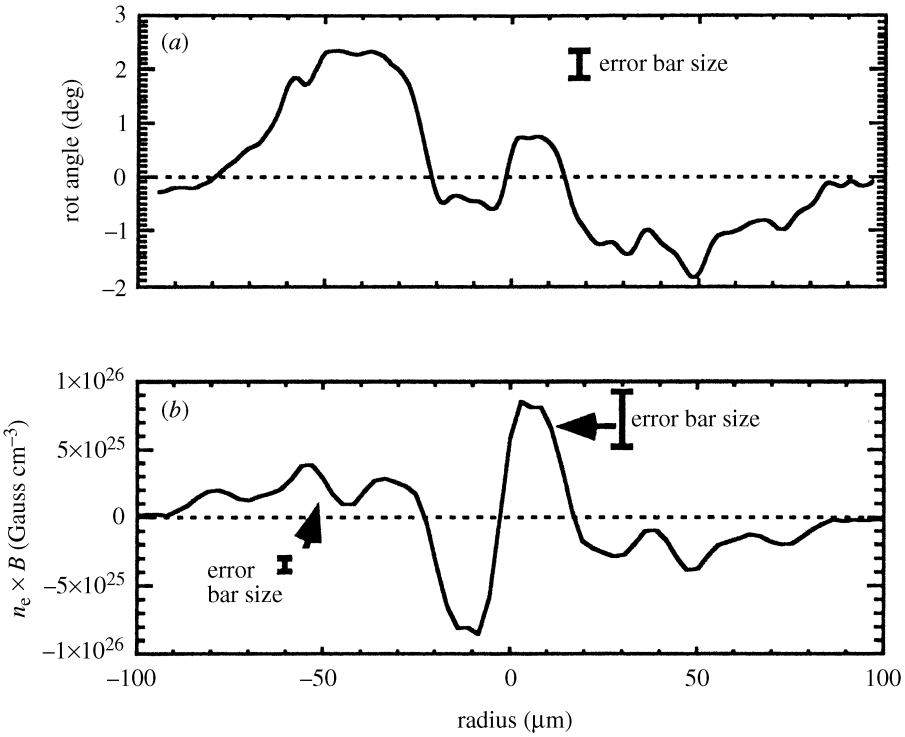

Figure 5. (*a*) Faraday rotation angle obtained by microdensitometry from experimental data. (*b*) Lineout of nB (density times magnetic field) extracted by Abel inversion from the trace of (*a*).

At a background density of $0.1n_c$, the magnetic field is predicted to be as large as 9 MG, peaking at a distance of 4–5 μm from the laser axis. In the predicted density profile, one observes that the beam has formed a hollow cylinder type of depression, with outgoing shocks and a density maximum on axis (Borghesi *et al.* 1998*a*).

The formation of a channel at densities higher than critical (*hole boring*) is a fundamental requirement of the fast ignitor scheme, since it will allow the ignitor pulse to be absorbed close to the core, resulting in an efficient coupling of the fast electron energy to the compressed fuel. Two-dimensional PIC simulations have been carried out with a 10× critical density plasma showing hole boring and the formation of an overdense channel (Pukhov & Meyer-ter-Vehn 1997). The channel is surrounded by a magnetic field of the order of 100 MG. Recent simulations with a hybrid code in which the hot electrons are treated as particles and the background as a fluid with collision taken into account also show an electron beam collimated by the self-generated magnetic field (Davis *et al.* 1999). In this case, however, the magnitude of the self-generated magnetic field was only a few megagauss. These simulations were carried out with a solid density plasma. So far, relatively little experimental evidence has been obtained that clearly demonstrates hole boring. The most convincing data of hole boring so far are observations of redshifted reflected harmonic emission indicating an inward motion of the critical density surface (Zepf *et al.* 1996; Kodama *et al.* 1996).

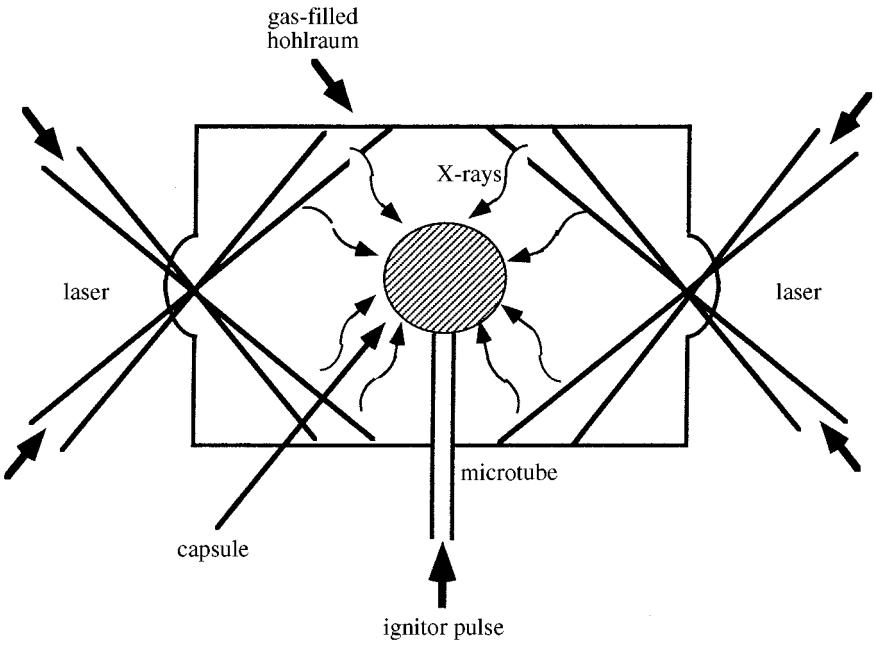

Figure 6. A microtube is used to guide the ignitor pulse through the wall and the underdense plasma of a gas-filled hohlraum target.

(*d*) *Guiding of the ignitor pulse through a microtube*

An alternative approach to the plasma channel formation and guiding not yet widely investigated is the use of hollow capillary tubes. In this case the laser pulse is confined within the inner diameter of the guide and propagates through reflections off the inner walls of the tube. Microtubes also allow an investigation of the interaction of an intense laser pulse with channel walls with steep density gradients, as in an overdense channel. The propagation of laser pulses with a power up to 1 TW through glass microcapillary tubes (with diameters in the range 100–200 μm) was first studied by Jackel *et al*. (1995). For energies below the breakdown threshold, the propagation occurs through grazing incidence reflections at the dielectric inner surface, the reflectivity for each bounce being determined by Fresnel laws. For high intensity pulses, however, an overdense plasma is created at the guide walls ahead of the main pulse, by the pulse's rising edge or by the prepulse. In this case the beam is guided through reflections off the high-density plasma. Since in principle some energy is absorbed by the plasma at every bounce, a reflection coefficient R can be introduced. The total transmission through the guide will be $T \approx T_{\mathrm{ins}}(R)^N$, where the insertion coefficient T_{ins} represents the fraction of the pulse energy that can be coupled to the guide and N is the number of bounces undergone by the pulse along the length of the guide. Guiding of high-intensity pulses through solid guides appears to be of particular interest in view of fast ignition. In principle, the igniting pulse can be guided to the high-density core of an imploding target, or at least through the coronal plasma region, in a solid waveguide, provided its walls are thick enough to survive the compression. This approach, in principle also applicable to direct-drive compression schemes, seems particularly promising for point ignition

following indirect-drive compression of a pellet placed inside a hohlraum. In this case, in order to reach the compressed core, the igniting pulse can be guided inside a hollow capillary tube through the hohlraum wall and the gas fill as shown in figure 6. Considering the size of hohlraums presently in use, the guide lengths of interest for these applications are in the 1–10 mm range. Efficient guiding of 1 ps infrared laser pulses with power exceeding 10 TW has been demonstrated through hollow capillary tubes with 40 and 100 μm internal diameters and lengths up to 10 mm, with transmittivity higher than 80% of the incident energy (Borghesi *et al.* 1998*b*). The beam is guided via multiple reflections off a plasma formed on the walls of the guide by the pulse's rising edge, as inferred from optical probe measurements.

5. Hot-electron production and propagation

Once the channel has been bored through the plasma, the hot electrons produced at critical density must propagate to the high-density core and deposit their energy. As a multi-kilojoule electron pulse is required for ignition it is essential that the laser energy is absorbed and converted into hot electrons efficiently. These electrons have to propagate through the dense plasma in a collimated beam and deposit their energy in a localized spot in the fusion fuel.

(*a*) *Laser absorption and hot-electron yield*

There are several processes that absorb laser energy in steep density gradients. Inverse bremsstrahlung is not very effective in plasmas with steep gradients, hence most of the laser energy is absorbed via resonance absorption, classical and anomalous skin effects (Gamaly 1990), vacuum (Brunel 1987; Gibbon & Bell 1992) and $\boldsymbol{J}\times\boldsymbol{B}$ heating (Denavit 1992; Wilks 1993; Ruhl & Mulser 1995). Absorption fractions between 30 and 50% were measured over a wide variety of conditions in agreement with PIC code simulations. Several experiments have recently been carried out to investigate the production of hot electrons with picosecond laser pulses. The energy conversion in hot electrons has been indirectly measured in various experiments at irradiances up to 10^{19} W cm^{-2}, by observing the X-rays produced by the electrons through bremsstrahlung and K_α emission. Conversion efficiencies of the laser energy in hot electrons in the range 10–50% have been reported (Key *et al.* 1998). In addition, a series of PIC simulations show similar conversion efficiencies.

(*b*) *Hot-electron temperature*

The production of energetic MeV electrons is required. The longitudinal oscillating component of the relativistic ponderomotive force will accelerate electrons to large velocities twice in every cycle. Electrons escape from the field with an average kinetic energy $W_{\mathrm{osc}} = (\gamma - 1)m_0c^2$. Assuming a Maxwellian hot-electron distribution, the hot-electron temperature T_{h} [MeV] $= 0.5((1+I\lambda^2/1.37\times10^{18})^{1/2}-1)$, where I is the laser irradiance in W cm^{-2} and λ is the laser wavelength in μm. In the relativistic regime, the Lorentz component of the force by an electron in an electromagnetic wave becomes comparable to the electric field. The electrons follow a figure-of-eight orbit in the average rest frame. It follows that the electrons are accelerated directly by the laser wave along the direction of propagation. In addition, stimulated Raman

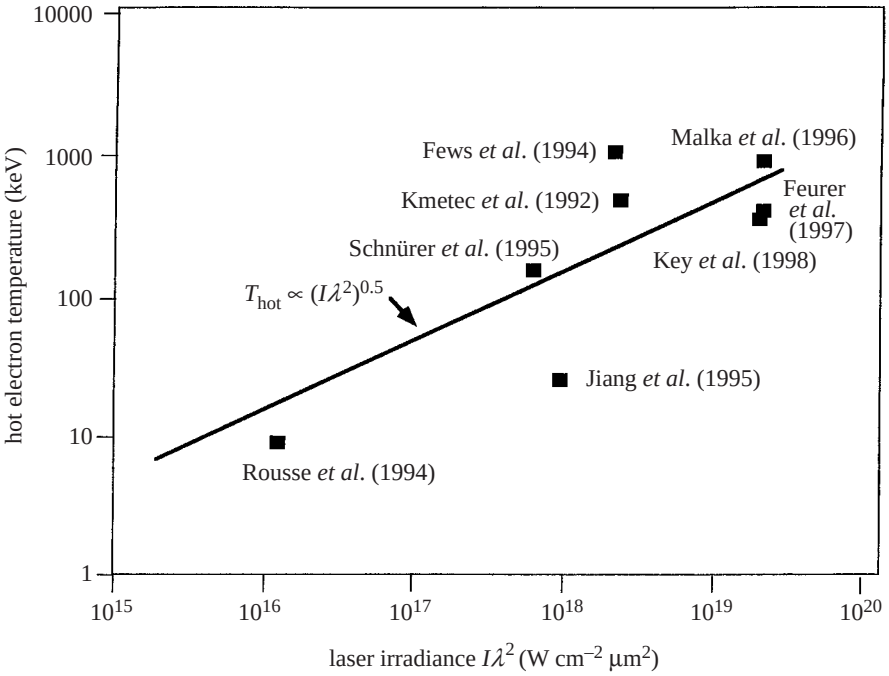

Figure 7. Hot-electron temperature scaling with $I\lambda^2$.

forward scattering can contribute to the acceleration of the electrons in the underdense plasma (Kruer 1988). The transport of the hot electrons through the overdense plasma may be limited as the plasma conductivity may not be high enough for an adequate return current (Bell *et al.* 1997).

The hot-electron temperature in short pulse experiments has recently been inferred from several different diagnostics including bremsstrahlung and K_α emission (Rousse *et al.* 1994; Jiang *et al.* 1995; Schnürer *et al.* 1995; Kmetec *et al.* 1992; Feurer *et al.* 1997), the detection of MeV ions (Fews *et al.* 1994) and electron spectroscopy (Malka & Miquel 1996; Malka *et al.* 1997). The electron temperature was found to follow the ponderomotive potential of the laser for those electrons directed along the axis of the laser beam in the interaction of preformed plasmas (Malka *et al.* 1997). A population of electrons with an energy larger than 1 MeV was observed only when the intensity was above 5×10^{18} W cm^{-2}. A pronounced directionality in the forward direction (laser pulse) was observed (Key *et al.* 1998) in the bremsstrahlung emission measurements produced by hot electrons.

Figure 7 shows a summary of several hot-electron measurements in short-pulse experiments.

(*c*) *Deposition of electron energy in compressed matter*

Experimental measurements have recently been carried out to measure the hot-electron deposition in shock-compressed matter by using K_α spectroscopy as a diagnostic. An increase of the K_α yield was observed in the compressed matter (Hall *et al.* 1998).

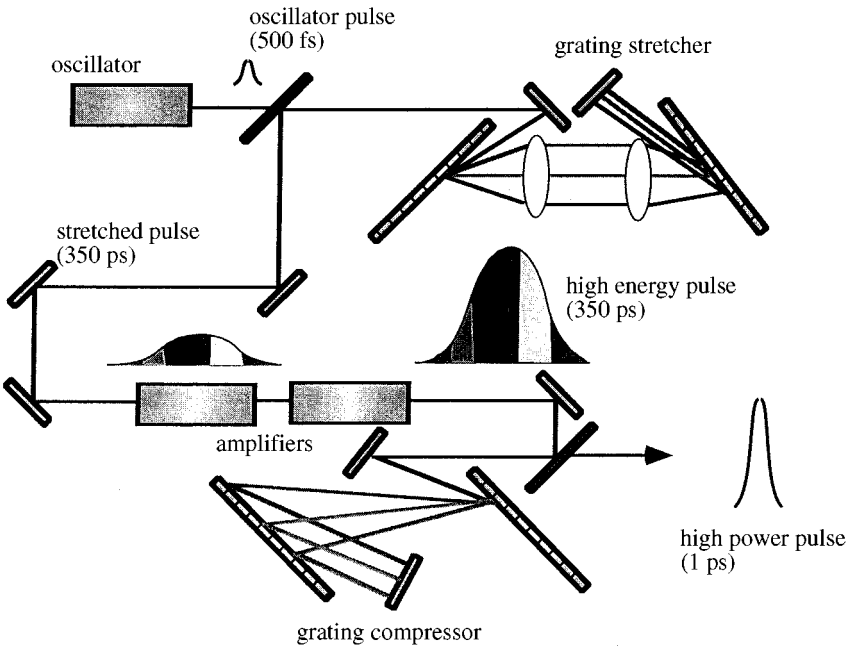

Figure 8. A schematic of a typical CPA laser system.

An analytical model has recently been developed to predict the interaction of the relativistic electrons with the precompressed thermonuclear fuel (Deutsch *et al.* 1996). The energy loss to the target electrons is treated through binary collisions and Langmuir wave excitations. The maximum penetration depth is determined by quasi-elastic and multiple scattering by target ions. For a 5 keV plasma compressed to a density of 300 g cm^{-3} a maximum penetration depth of about 10 μm is predicted for 1 MeV electrons. This range reduces to about 3 μm when the plasma is compressed up to a density of 1000 g cm^{-3}. The electron temperature must not exceed an energy of a few MeV, otherwise the deposition range becomes too large. For high conversion efficiencies a large $I\lambda^2$ is important. Consequently, a shorter laser wavelength may result in a high conversion efficiency and also in a hot-electron temperature that is not too large.

6. Generation of picosecond laser pulses

The feasibility of fast ignition relies on technical progress that has only recently been made. Peak laser powers up to 1 PW have now been demonstrated with the NOVA laser at the Lawrence Livermore National Laboratory with laser energies of 500 J in a 500 fs laser pulse exceeding irradiances of 10^{20} W cm^{-2} on target. There are also smaller systems at CEA-Limeil in France, Ecole Polytechnique in Paris, Rutherford Appleton Laboratory in the UK, ILE-Osaka in Japan with powers between 50 and 100 TW.

The increase in peak power and irradiance have been the direct result of chirped pulse amplification (CPA) (Maine *et al.* 1988). At picosecond pulse duration it is difficult to extract the stored energy from the laser amplifier without causing catastrophic damage to the amplifier glass. The input pulse fluence needed to efficiently

Table 1. *Present understanding of some of the fast ignitor physics issues*

channel formation	in the underdense plasma	extensive experimental data in agreement with theory
	in the overdense plasma	extensive theoretical models but very few experimental data
ignition pulse guiding		preliminary experimental results at irradiances $> 10^{19}$ W cm^{-2}
electron beam production		extensive experimental data, but consistent picture still has to emerge
propagation of electron beam		preliminary experimental results (unpublished) agreeing with theory
electron beam deposition at high densities		only theoretical work
ignition		only theoretical work

extract energy from the amplifier is given by the saturation fluence. The saturation fluence of most solid-state materials is between 1 and 6 J cm^{-2}. Amplification of picosecond pulses is not possible because of the intensity-dependent index of refraction ($n = n_0 + n_2 I$) that produces a nonlinear phase retardation given by the B integral

$$B = \frac{2\pi}{\lambda} \int_0^L n_2 I(z)\, \mathrm{d}z,$$

where L is the propagation length. This nonlinear retardation results in wavefront distortion and eventually filamentation and self-focusing in the amplifier glass. To amplify a subpicosecond laser pulse efficiently in solid state the pulse must be stretched by a factor of several hundreds or more before amplification. The broadband oscillator pulse, typically subpicosecond in duration is stretched by double passing it through a pair of gratings. By using the dispersive properties of the gratings, the pulse is chirped in frequency and the duration is typically increased to a few hundred picoseconds. The pulse is now amplified by a factor of 10^6–10^{10} without damaging the amplifiers and allows efficient energy extraction from the amplifiers without incurring nonlinear effects associated with high intensity. The recompression to a picosecond or subpicosecond duration is then performed with a second pair of gratings. Figure 8 shows a schematic of the CPA laser system. The actual limit in the power output of CPA laser systems is fixed by the damage threshold and the size of available gratings. Gratings with a damage threshold up to 3 J cm^{-2} and a diffraction efficiency of more than 90% have been developed at the Lawrence Livermore National Laboratory (Perry & Mourou 1994). The gratings for the petawatt laser system are typically 1 m in diameter.

7. Summary and conclusions

This paper reviewed some of the critical issues relevant for the fast ignitor concept. The physical processes involved are not yet well understood as this area of research takes place in a novel parameter regime. Several laser laboratories have now multiterawatt short pulse CPA laser systems. In addition, several university laboratories have built terawatt lasers. Sophisticated computer codes have been developed during the past few years to design and model experimental studies. If the fast ignitor scheme

proves to be successful it will have a major impact in IFE as substantially higher gains are achieved at lower driver energies as obtained with the present conventional spark ignition. There are, however, major physics issues that have to be investigated before clear conclusions can be drawn. In the past few years, encouraging results have been obtained both computationally and experimentally. A number of experimental studies have been published confirming light channelling, the onset of hole boring under the action of light pressure observing the inward motion of the critical surface via redshifted light, the generation of MeV electrons with a two-temperature distribution, the observation of X-ray produced by the relativistic electrons through bremsstrahlung and the production of thermal neutrons. The present understanding of some of the major physics issues of the fast ignitor concept is briefly summarized in table 1.

I thank Dr S. Atzeni, Dr A. Pukhov and Dr M. Key for providing data even before they were published, and Marco Borghesi for helping to prepare the figures.

References

Askar'yan, G. A., Bulanov, S. V., Pegoraro, F. & Pukhov, A. M. 1995 *Plasma Phys. Rep.* **21**, 835.

Atzeni, S. 1995 *Jpn. J. Appl. Phys.* **34**, 1980.

Atzeni, S. & Ciampi, M. L. 1997 *Nucl. Fusion* **37**, 1665.

Atzeni, S., Ciampi, M. L. & Piriz, A. R. 1997 In *Advances in laser interaction with matter and inertial fusion* (ed. G. Velarde, J. M. Martinez-Val, E. Minguez & J. M. Perlado), p. 275. Singapore: World Scientific.

Bell, A. R., Davies, J. R., Guerin, S. & Ruhl, H. 1997 *Plasma Phys. Control. Fusion* **39**, 653.

Borghesi, M., MacKinnon, A. J., Barringer, L., Gaillard, R., Gizzi, L. A., Meyer, C., Willi, O., Pukhov, A. & Meyer-ter-Vehn, J. 1997 *Phys. Rev. Lett.* **78**, 879.

Borghesi, M., MacKinnon, A. J., Gaillard, R., Willi, O., Pukhov, A. & Meyer-ter-Vehn, J. 1998*a* *Phys. Rev. Lett.* **80**, 5137.

Borghesi, M., MacKinnon, A. J., Gaillard, R., Willi, O. & Offenberger, A. 1998*b* *Phys. Rev.* E **57**, R4899.

Brunel, F. 1987 *Phys. Rev. Lett.* **59**, 52.

Burnett, N. H. & Enright, G. D. 1990 *IEEE J. Quantum Electron* **24**, 398.

Chen, F. F. 1984 *Introduction to plasma physics and controlled fusion*. New York: Plenum Press.

Davis, J., Bell, A. & Tatarakis, M. 1999 *Phys. Rev.* (In the press.)

Denavit, J. 1992 *Phys. Rev. Lett.* **69**, 3052.

Deutsch, C., Furukawa, H., Mima, K., Murakami, M. & Nishihara, K. 1996 *Phys. Rev. Lett.* **77**, 2483.

Feurer, T., Theobald, W., Sauerbrey, R., Uschmann, I., Altenbernd, D., Teubner, U., Gibbon, P., Forster, E., Malka, G. & Miquel, J. L. 1997 *Phys. Rev.* E **56**, 4608.

Fews, A. P., Norreys, A. P., Beg, F. N., Bell, A. R., Dangor, A. E., Danson, C. N., Lee, P. & Rose, S. J. 1994 *Phys. Rev. Lett.* **73**, 1801.

Forslund, D. W. 1985 *Phys. Rev. Lett.* **54**, 558.

Fuchs, J. (and 11 others) 1998 *Phys. Rev. Lett.* **80**, 1658.

Gamaly, E. G. 1990 *Phys. Rev.* A **42**, 929.

Gibbon, P. & Bell, A. R. 1992 *Phys. Rev. Lett.* **68**, 1535.

Gibbon, P. & Förster, E. 1996 *Plasma Phys. Control. Fusion* **38**, 769.

Hall, T. A. (and 14 others) 1998 *Phys. Rev. Lett.* **81**, 1003.

Jackel, S., Burris, R., Grun, J., Ting, A., Manaka, C., Evans, K. & Kosakowskii, J. 1995 *Opt. Lett.* **20**, 1086.

Jiang, Z., Kieffer, J. C., Matte, J. P., Chaker, M., Audebert, P., Pepin, H., Maine, P., Strickland, D., Bado, P. & Mourou, G. 1995 *Phys. Plasmas* **2**, 1702.

Kaw, P. & Dawson, J. 1970 *Phys. Fluids* **13**, 472.

Key, M. H. (and 29 others) 1998 *Phys. Plasmas* **5**, 1966.

Kidder, R. 1976 *Nucl. Fusion* **16**, 405.

Kidder, R. 1979 *Nucl. Fusion* **19**, 223.

Kmetec, J. D., Gordon, C. L., Macklin, J. J., Lemoff, B. E., Brown, S. G. & Harris, S. E. 1992 *Phys. Rev. Lett.* **68**, 1527.

Kodama, R., Takahashi, K., Tanaka, K. A., Tsukamoto, M., Hashimoto, M., Kato, Y. & Mima, K. 1996 *Phys. Rev. Lett.* **77**, 4906.

Kruer, W. L. 1988 *The physics of laser–plasma interaction*. Redwood City, CA: Addison-Wesley.

Kruer, W. L. & Wilks, S. C. 1994 In *Advances in plasma physics*. Woodbury, NY: AIP.

Krushelnick, K., Ting, A., Moore, C. I., Burris, H. R., Esarey, E., Sprangle, P. & Baine, M. 1997 *Phys. Rev. Lett.* **78**, 4047.

Maine, P., Strickland, D., Bado, P., Pessot, M. & Mourou, G. 1988 *IEEE J. Quantum Electron* QE **24**, 398.

Malka, G. & Miquel, J. L. 1996 *Phys. Rev. Lett.* **77**, 75.

Malka, G., Fuchs, J., Amiranoff, F., Baton, S. D., Gaillard, R., Miquel, J. L., Pepin, H., Rousseaux, C., Bonnaud, G., Busquet, M. & Lours, L. 1997 *Phys. Rev. Lett.* **79**, 2055.

Mason, R. J. & Tabak, M. 1998 *Phys. Rev. Lett.* **80**, 524.

Meyer-ter-Vehn, J. 1982 *Nucl. Fusion* **22**, 561.

Meyer-ter-Vehn, J. 1997 *Plasma Phys. Control. Fusion* **39**, B39.

Mori, W. B., Joshi, C., Dawson, J. M., Forslund, D. W. & Kindel, J. M. 1988 *Phys. Rev. Lett.* **60**, 1298.

Nuckolls, J., Wood, L., Thiessen, A. & Zimmermann, G. 1972 *Nature* **239**, 139.

Pegoraro, F., Bulanov, S. V., Califano, F. & Lontano, M. 1996 *Physica Scr.* T **63**, 262.

Perry, M. D. & Mourou, G. 1994 *Science* **264**, 917.

Pukhov, A. & Meyer-ter-Vehn, J. 1996 *Phys. Rev. Lett.* **76**, 3975.

Pukhov, A. & Meyer-ter-Vehn, J. 1997 *Phys. Rev. Lett.* **79**, 2686.

Rousse, A., Audebert, P., Geindre, J. P., Fallies, F., Gauthier, J. C., Mysyrowicz, A., Grillon, G. & Antonetti, A. 1994 *Phys. Rev.* E **50**, 2200.

Ruhl, H. & Mulser, P. 1995 *Phys. Lett.* A **205**, 388.

Schnürer, M., Kalashnikov, M. P., Nickles, P. V., Schlegel, Th., Sandner, W., Demchenko, N., Nolte, R. & Ambrosi, P. 1995 *Phys. Plasmas* **2**, 3106.

Sedov, L. I. 1959 *Similarity and dimensional methods in mechanics*. New York: Academic Press.

Sprangle, P., Esarey, E., Krall, J. & Joyce, G. 1992 *Phys. Rev. Lett.* **69**, 15.

Sun, G. Z., Ott, E., Lee, Y. C. & Guzdar, P. 1987 *Phys. Fluids* **30**, 526.

Tabak, M., Hammer, J., Glinsky, M., Kruer, W. L., Wilks, S. C. & Langdon, A. B. 1994 *Phys. Plasmas* **1**, 1626.

Taylor, G. I. 1950 *Proc. R. Soc. Lond.* A **201**, 192.

Wagner, R., Chen, S. Y., Maksimchuk, A. & Umstadter, D. 1997 *Phys. Rev. Lett.* **78**, 3125.

Weibel, E. S. 1959 *Phys. Rev. Lett.* **2**, 83.

Wilks, S. C. 1993 *Phys. Fluids* B **5**, 2603.

Wilks, S. C., Kruer, W. L., Tabak, M. & Langdon, A. B. 1992 *Phys. Rev. Lett.* **69**, 1383.

Young, P. E. & Bolton, P. R. 1996 *Phys. Rev. Lett.* **77**, 4556.

Zepf, M. (and 15 others) 1996 *Phys. Plasmas* **3**, 3242.

PHILOSOPHICAL TRANSACTIONS OF THE ROYAL SOCIETY A MATHEMATICAL, PHYSICAL & ENGINEERING SCIENCES

Discussion

D. C. Robinson (*UKAEA Fusion, Culham Science Centre, Abingdon, UK*). There is clearly some interesting physics here. What is the position of instabilities created by the generated magnetic fields and filamentation, and will these affect the ability to propagate the fast pulse down the channel to the core? How would what is going on in the overdense plasma be measured?

O. Willi. The simulations show that the channel in the overdense plasma is stable. XUV probing including Faraday rotation will be used to study the channel in the overdense plasma with sources such as higher harmonics and soft X-ray lasers.

J. D. Lawson (*Abingdon, UK*). If fast ignition is used in a reactor, is the lining up and timing of the pellet more critical than for a conventional target?

O. Willi. The alignment accuracy has to be within 100 μm, so that the electron beam pulse will hit the compressed fuel region.

E. A. Little (*University of Wales, Swansea, UK*). One of the simulations attributed to the Frascati group showed the burn/ignition of a cylindrical pellet that appears to be more efficient than that of a spherical pellet. Would Dr Willi advocate a change of pellet geometry, and would the cylindrical format be the optimum, or are other geometries likely to be explored?

O. Willi. Virtually all of research so far has concentrated on spherical targets. With the fast ignition concept, different geometries can now be used, in particular cylindrical targets. Certainly, computational studies should be done to optimize the geometry.

S. Zweben (*PPPL, Princeton, USA*). The burn propagation analysis Dr Willi showed was two dimensional. Is it clear that the burn will be efficient and stable in three dimensions, particularly considering possible asymmetries in the target?

O. Willi. No simulations have been carried out in three dimensions so far. There could be asymmetries in the burn-wave propagation.

T. N. Todd (*D3, UKAEA Fusion, Culham Science Centre, Abingdon, UK*). Dr Willi appeared to say in answer to an earlier question (by Dr Robinson) that the relativistic electron channel did not exhibit MHD instabilities. How then should I interpret the apparent $m = 0$ (sausage) instability shown in the 2D and 3D (experimental and modelling) views of the channel?

O. Willi. The self-emission image shows pulsations in the width of the channel. This is caused by laser diffraction and self-focusing.